# Supporting Information

## Length-tunable $Pd_2Sn$@Pt core-shell nanorods for enhanced ethanol electrooxidation with concurrent hydrogen production

Tong Li, Qiuxia Wang, Wenjie Zhang, Huaming Li, Yong Wang*, Junfeng Liu*

Institute for Energy Research, School of Chemistry and Chemical Engineering, Jiangsu University, Zhenjiang 212013, China

Email: wangyong@ujs.edu.cn (Y. Wang); jliu@ujs.edu.cn (J. Liu)

**Chemicals.**

Palladium(II) acetylacetonate ($Pd(acac)_2$, 98%), and Nafion (10 wt% in water) were obtained from Sigma-Aldrich. Tin(II) acetate ($Sn(OAc)_2$, 95.3%) and methylamine hydrochloride (MAHC) were purchased from Bide Pharmatech Ltd. A commercial Pt on carbon catalyst (Pt/C, 20% Pt) was purchased from Alfa Aesar. Glucose was obtained from Sinopharm Chemical Reagent Co., Ltd. Chloroplatinic acid hexahydrate ($H_2PtCl_6 \cdot 6H_2O$) and oleylamine (OAm, approximate C18 content 80-90%) were purchased from Macklin. Ammonium thiocyanate ($NH_4SCN$, 99.99%) was obtained from Rhawn. Trioctylphosphine (TOP, 90%) was obtained from Shanghai Aladdin Biochemical Technology Co., Ltd. Potassium hydroxide, chloroform and ethanol were of analytical grade and purchased from Sinopharm Chemical Reagent Co. Ltd. All reagents were used as received without further purification.

**Synthesis of $Pd_2Sn$ NRs.**

All reactions were conducted under a nitrogen atmosphere employing standard Schlenk line techniques. In a typical synthesis, 91.4 mg (0.3 mmol) of $Pd(acac)_2$, 37.6 mg (0.15 mmol) of $Sn(OAc)_2$, 20 mL of OAm, 1 mL of TOP, and a certain amount of MAHC were introduced into a 50 mL three-necked flask equipped with a thermocouple and its adapter, a condenser, and a septum. The system was heated to 60 °C under nitrogen and maintained at this temperature for 30 min to eliminate moisture, oxygen and low-boiling point impurities. Subsequently, the temperature was increased to 200 °C within 10 min and held at this temperature for 30 min. Then, the temperature was further

increased to 300 °C over 40 min and maintained for an additional 30 min. Afterward, the mixture was allowed to cool to ambient temperature naturally. The resulting black product was transferred to centrifuge tubes and subjected to centrifugation at 8000 rpm for 5 min. Purification was achieved by performing dispersion/precipitation steps twice using chloroform and ethanol.

**Synthesis of spherical $Pd_2Sn$ nanoparticles.**

In a typical synthesis, 91.4 mg (0.3 mmol) of $Pd(acac)_2$, 37.6 mg (0.15 mmol) of $Sn(OAc)_2$, 20 mL of OAm and 1 mL of TOP were introduced into a 50 mL three-necked flask. The system was heated to 60 °C under nitrogen and maintained at this temperature for 30 min. Subsequently, the temperature was increased to 200 °C within 10 min and held at this temperature for 30 min. Then, the temperature was further increased to 300 °C over 40 min and maintained for an additional 30 min. The purification steps utilized for $Pd_2Sn$ NRs were identical and applied in this case as well.

**Synthesis of $Pd_2Sn$@Pt.**

In a typical synthesis, $Pd_2Sn$ NRs or spherical $Pd_2Sn$ nanoparticles were dispersed in a 50 mL three-necked flask containing 20 mL of OAm. Then, 25 mg of $H_2PtCl_6 \cdot 6H_2O$ and 125 mg of glucose monohydrate were added into the flask under magnetic stirring. The reaction mixture was purged with nitrogen at 60 °C for 10 min, followed by increasing the reaction temperature to 200 °C within 10 min. The temperature was maintained at 200 °C for 30 min before the mixture was allowed to cool down to ambient temperature. The resultant precipitate was isolated through centrifugation at

8000 rpm for 5 min. To minimize organic residues, multiple cycles of redispersion and precipitation were carried out using chloroform and ethanol. Finally, the obtained powder was suspended in chloroform until it was ready for further application.

**Characterization.**

X-ray diffraction (XRD) was performed on the sample supported on a silica glass substrate using a Bruker-AXS D8 X-ray diffractometer with Cu Kα radiation (λ = 1.5418 Å) operating at 40 kV and 40 mA. Transmission electron microscopy (TEM) characterization was carried out using a ZEISS LIBRA 120, operating at 120 kV and a JEOL 1011 operating at 100 kV. Carbon-coated TEM grids from Electron Microscopy China were used as substrates. High-resolution TEM (HRTEM) studies were conducted using a field emission gun FEI™ Tecnai F20 microscope at 200 kV. High angle annular dark-field scanning transmission electron microscope (HAADF-STEM) was performed on the Tecnai F20, by using a GATAN QUANTUM filter. High-performance liquid chromatography (HPLC) was performed using the Agilent 1260 Infinity system. Infrared transmission spectra were recorded using Nicolet iS50 FT-IR spectrometer in the range 4000-500 $cm^{-1}$. X-ray photoelectron spectroscopy (XPS) was analyzed on a Thermo Scientific K-Alpha XPS system equipped with an Al Kα source (hv = 1486.6 eV) operating at 12 kV and 6 mA, and binding energy values were referred to the adventitious C 1 s peak at 284.8 eV.

**Ligand exchange.**

The ligand exchange procedure utilized in this study followed a similar methodology

as previously reported by Fafarman et al.[1] In a typical procedure, 2 mL of 130 mM $NH_4SCN$ in acetone was added to 2 mL of a dispersion of as-synthesized nanomaterials in chloroform (approximately 5 mg in 2 mL). The solution was agitated for 1 minute, followed by centrifugation at 3000 rpm for 1 min. The resulting precipitate was then washed twice with chloroform and ethanol, respectively. Finally, the obtained precipitate was dried under ambient conditions.

**Preparation of Catalysts.**

The catalyst ink for electrochemical measurements was prepared by combining 1 mg of $Pd_2Sn$@Pt NRs, 4 mg of carbon black, 10 μL of 10% Nafion, 0.4 mL ethanol, and 0.6 mL of deionized water. The mixture was sonicated for 1 h to obatin a homogenous slurry. For comparison, the $Pd_2Sn$ ink or spherical $Pd_2Sn$@Pt ink was prepared by mixing 1 mg of $Pd_2Sn$ NRs or 1 mg of spherical $Pd_2Sn$@Pt with the same amount of carbon black, Nafion, ethanol and deionized water. The Pt/C ink was prepared using 5 mg of commercial Pt/C with the same amount of Nafion, ethanol and deionized water.

**Electrochemical measurements.**

Electrochemical measurements were performed using a CHI660E electrochemical workstation (CH Instruments Inc., Shanghai) at room temperature, employing a standard three-electrode system. A Hg/HgO (1 M KOH) electrode was used as the reference electrode, and a platinum mesh was served as the counter electrode. The working electrode was prepared by drop-casting 3.0 μL of the catalyst ink onto a glassy carbon electrode (GCE) with a diameter of 3 mm, followed by natural drying at room

temperature. For EOR measurement, cyclic voltammetry (CV) curves were recorded in aqueous solutions containing 1 M KOH and 1 M ethanol, scanning from -0.924 to 0.4 V versus Hg/HgO at a scan rate of 50 mV $s^{-1}$. Linear sweep voltammetry (LSV) tests were conducted at a scan rate of 10 mV $s^{-1}$. Chronoamperometry (CA) measurements were performed at a fixed potential of 0.724 V versus reversible hydrogen electrode (RHE) in a 1 M KOH + 1 M ethanol electrolyte. In the two-electrode measurement setup, the catalyst-modified GCE used as the anodic electrode, while a platinum mesh served as the cathodic electrode, and measured in a 1 M KOH + 1 M ethanol solution. All the electrochemical measurements were recorded and are presented without IR correction.

**Computational details.**

All calculations were carried out using the Vienna ab initio simulation package (VASP) code.[2,3] The Perdew-Burke-Ernzerhof functional with a generalized gradient approximation (GGA) was employed to describe the electronic exchange-correlation energy.[4,5] The projector augmented-wave was applied and the energy cutoff was 400 eV.[6] The sampling over Brillouin zone was treated by the Monkhorst-Pack type and k-point mesh with a 3 × 3 × 1 grid was introduced. The long-range van der Waals (vdW) interactions were taken into account using the DFT-D3 method with Becke-Johnson damping.[7,8] Geometry optimization was performed until convergence, defined as the maximal residual energy and force being less than $10^{-5}$ eV and -0.03 eV $Å^{-1}$, respectively. A vacuum slab of 15 Å was applied in z-direction to prevent pseudo interactions

between periodic units. The Pt (111) surfaces with four atomic layers or strain-tensile Pt (111) layers were chosen to construct the investigated periodic slab models. During the optimization, the top two layers were allowed to relax, while the remaining layers were fixed. Thermodynamic free energies were calculated using the formula $G = E_{DFT} + E_{ZPE} - TS$, where $E_{DFT}$ represents the DFT total energy, $E_{ZPE}$ is the zero-point energy, and TS denotes the entropy.

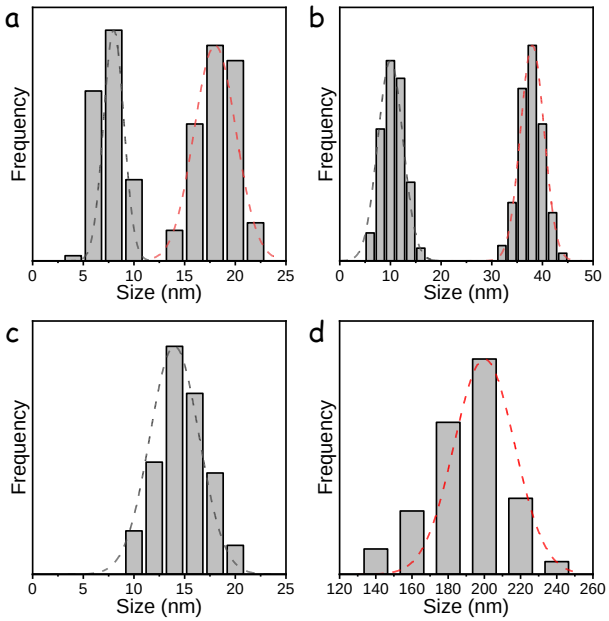


**Fig. S1.** Size distribution histogram of (a) $Pd_2Sn$-s@Pt, (b) $Pd_2Sn$-m@Pt, (c) the width of $Pd_2Sn$-l@Pt and (d) the length of $Pd_2Sn$-l@Pt.

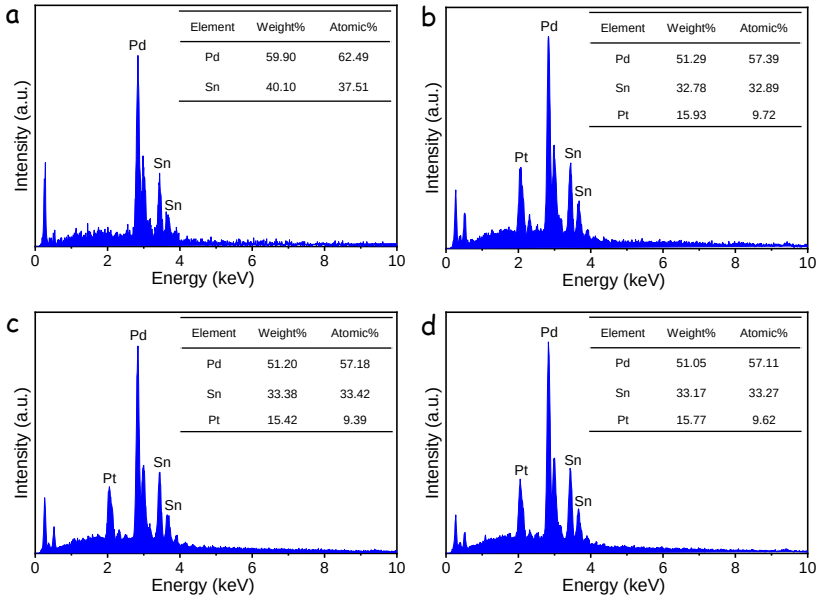


**Fig. S2.** EDS elemental composition of the (a) $Pd_2Sn$-s, (b) $Pd_2Sn$-s@Pt, (c) $Pd_2Sn$-m@Pt and (d) $Pd_2Sn$-l@Pt.

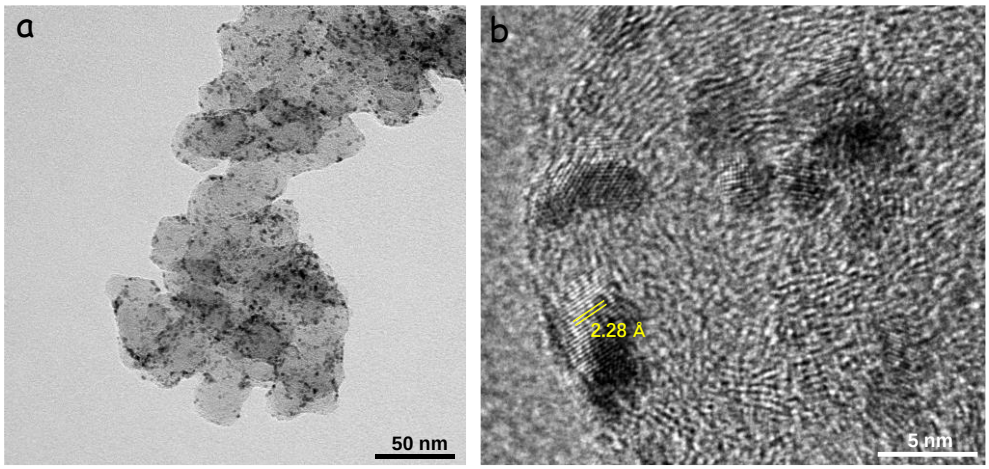


**Fig. S3.** (a) TEM and (b) HRTEM images of commercial Pt/C catalyst.

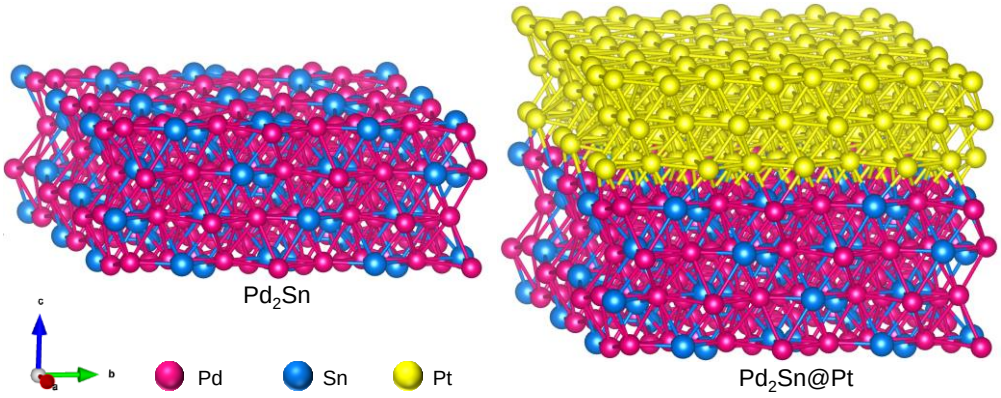


**Fig. S4.** Crystal structure models of $Pd_2Sn$ and $Pd_2Sn$@Pt.

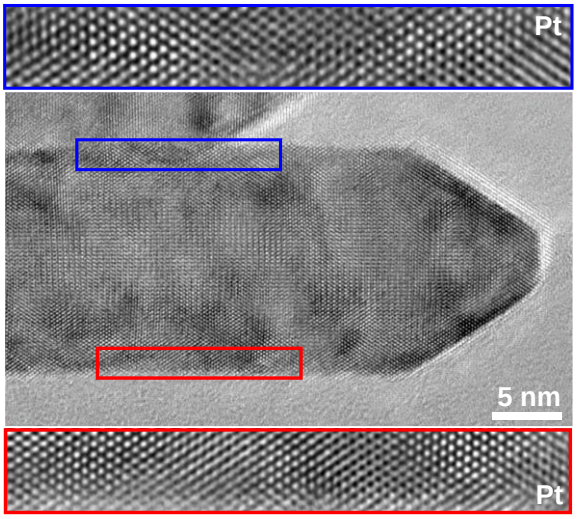


**Fig. S5.** HRTEM images of $Pd_2Sn$-l@Pt and integrated pixel intensity of the crystal phase taken from the blue and red rectangles.

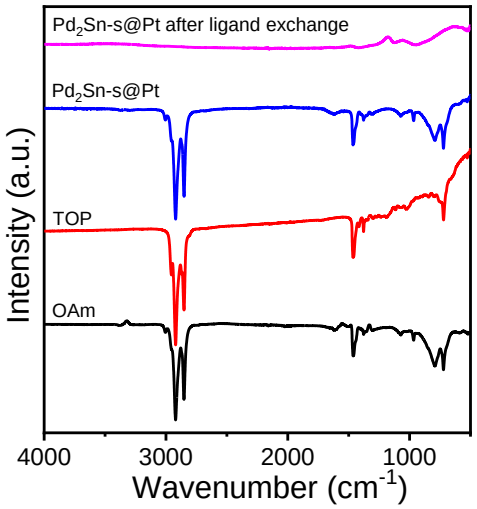


**Fig. S6.** FT-IR spectra of OAm, TOP, $Pd_2Sn$-s@Pt NRs and $Pd_2Sn$-s@Pt NRs after ligand exchange by $NH_4SCN$.

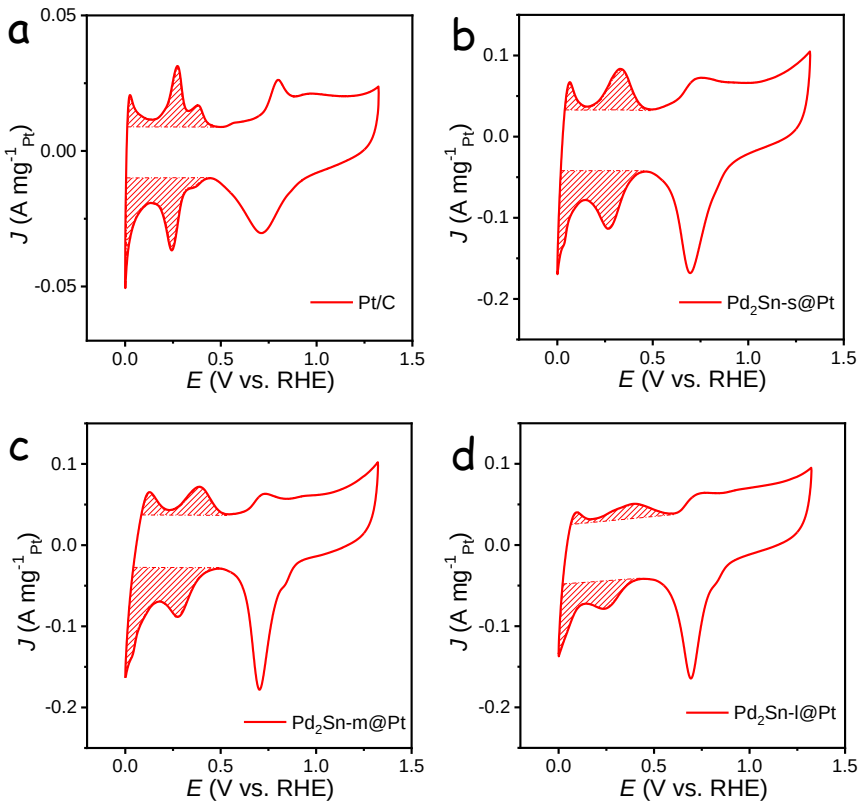


**Fig. S7.** Hydrogen adsorption/desorption for measuring the ECSA of (a) Pt/C, (b) $Pd_2Sn$-s@Pt, (c) $Pd_2Sn$-m@Pt and (d) $Pd_2Sn$-l@Pt catalysts.

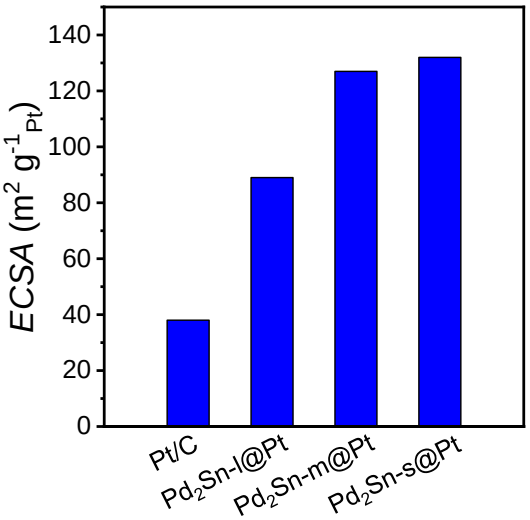


**Fig. S8.** The comparison of ECSA values of the catalysts.

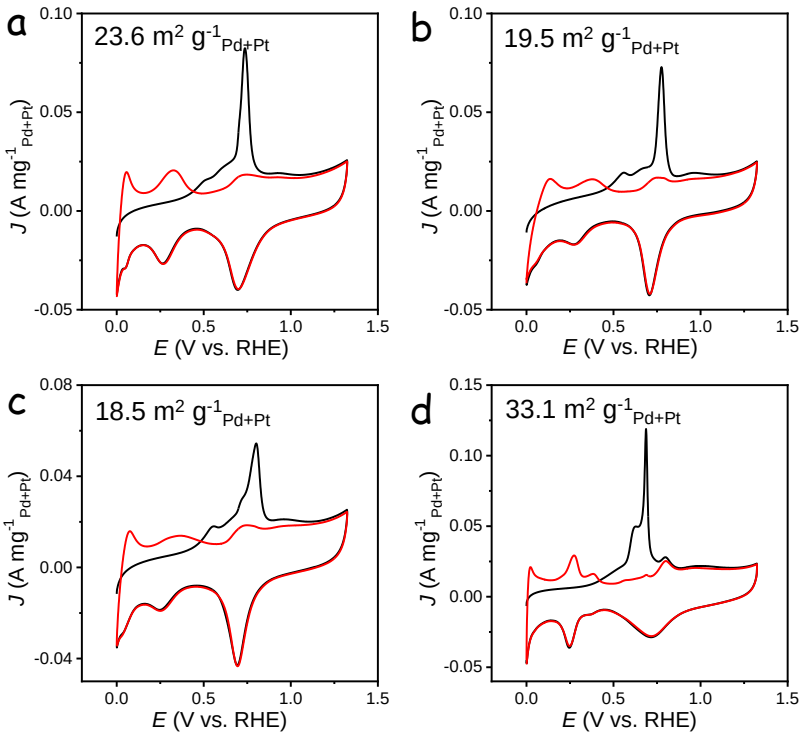


**Fig. S9.** CO stripping measurement of (a) $Pd_2Sn$-s@Pt, (b) $Pd_2Sn$-m@Pt, (c) $Pd_2Sn$-l@Pt and (d) Pt/C catalysts at 50 mV $s^{-1}$ in 1 M KOH + 1 M ethanol electrolyte that quantifies the surface area of ECSA.

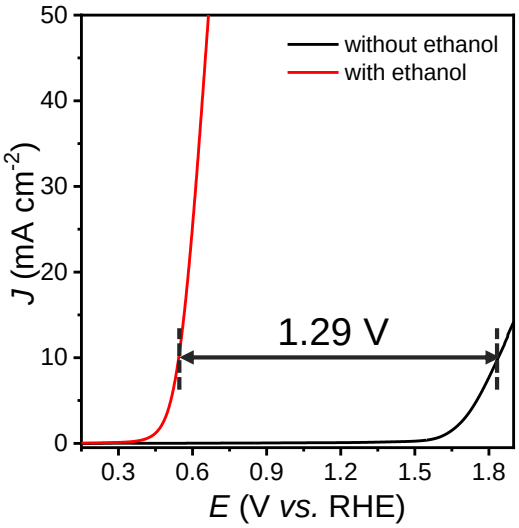


**Fig. S10.** LSV curves of $Pd_2Sn$-s@Pt in a 1 M KOH with and without 1 M ethanol.

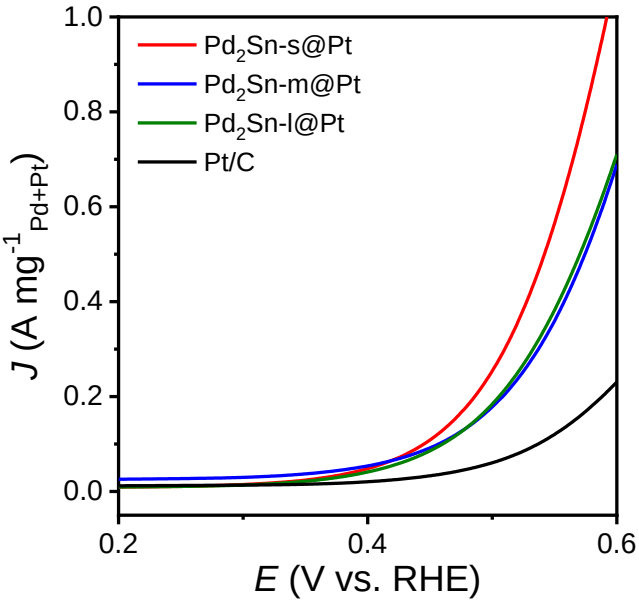


**Fig. S11.** LSV curves in the potential region from 0.2 to 0.6 V.

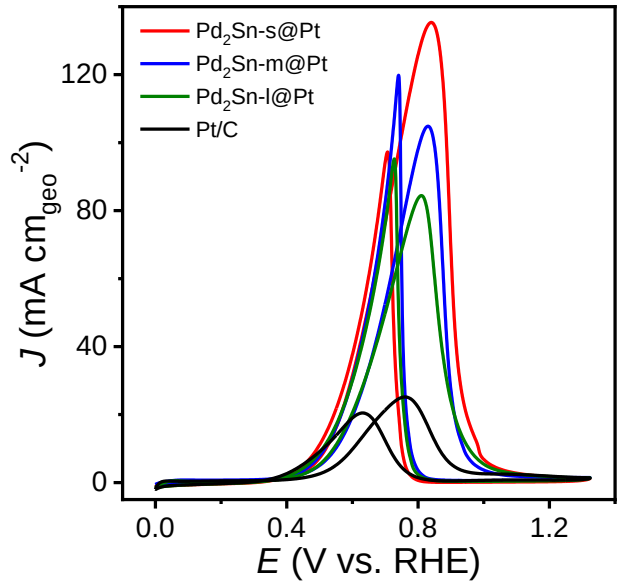


**Fig. S12.** CV curves of catalysts normalized to geometric area of electrode toward EOR in 1 M KOH with 1 M ethanol solution.

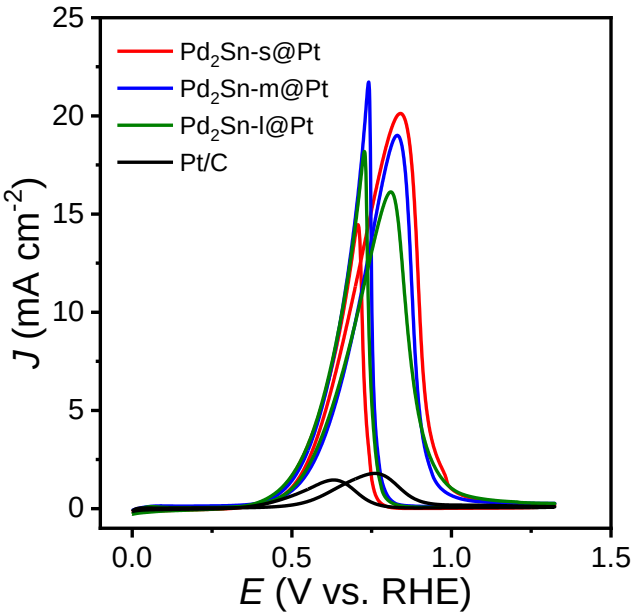


**Fig. S13.** CV curves of catalysts normalized to ECSA toward EOR in 1 M KOH with 1 M ethanol solution.

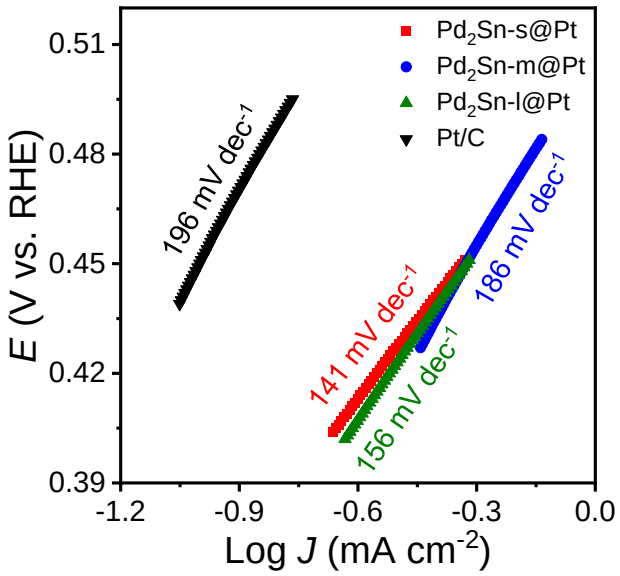


**Fig. S14.** Tafel plots of the catalysts calculated from CV curves in the potential range between 0.4 and 0.5 V.

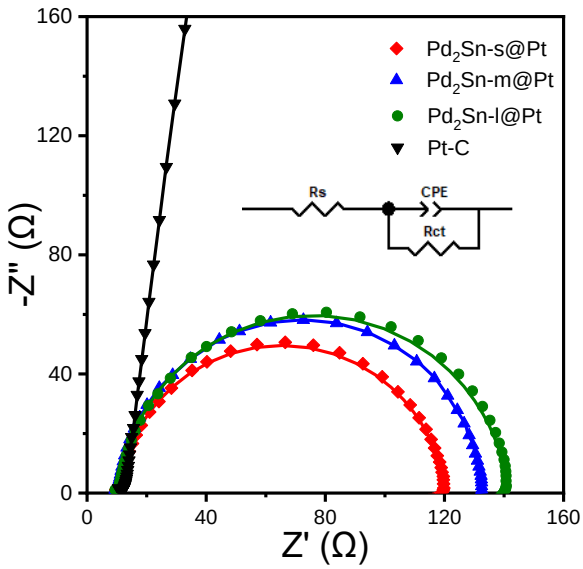


**Fig. S15.** Nyquist plots of the catalysts measured at -0.3 V vs. Hg/HgO in 1 M KOH with 1 ethanol solution.

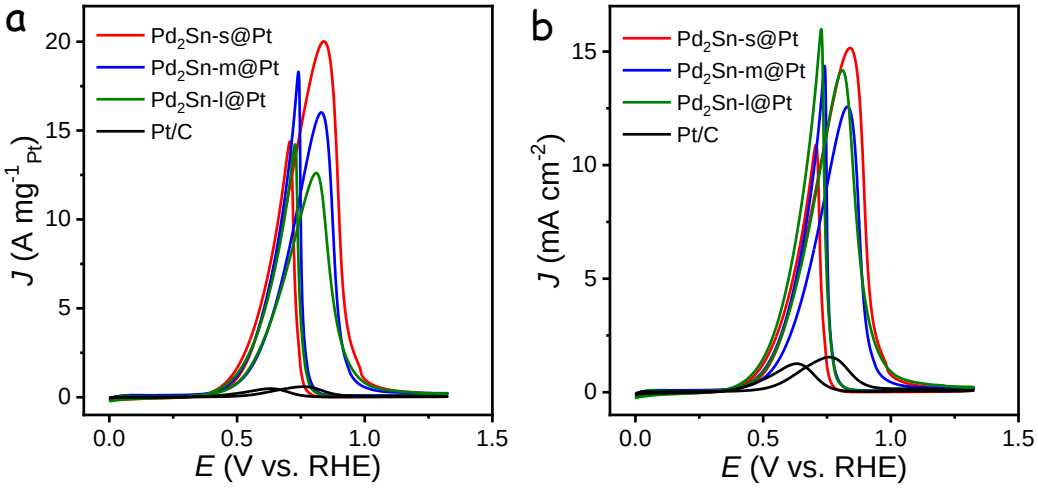


**Fig. S16.** CV curves of catalysts normalized to the amount of Pt mass and the corresponding ECSA toward EOR in 1 M KOH with 1 M ethanol solution.

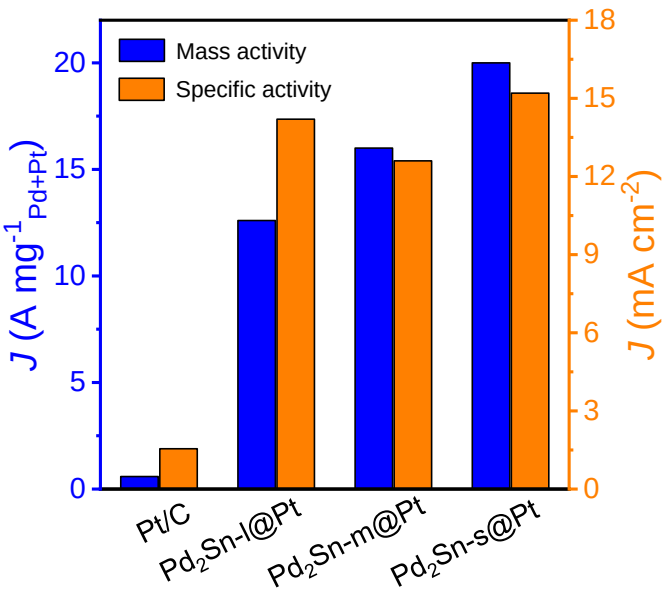


**Fig. S17.** The comparison of mass and specific activity of the catalysts normalized by the Pt mass and the corresponding ECSA, respectively.

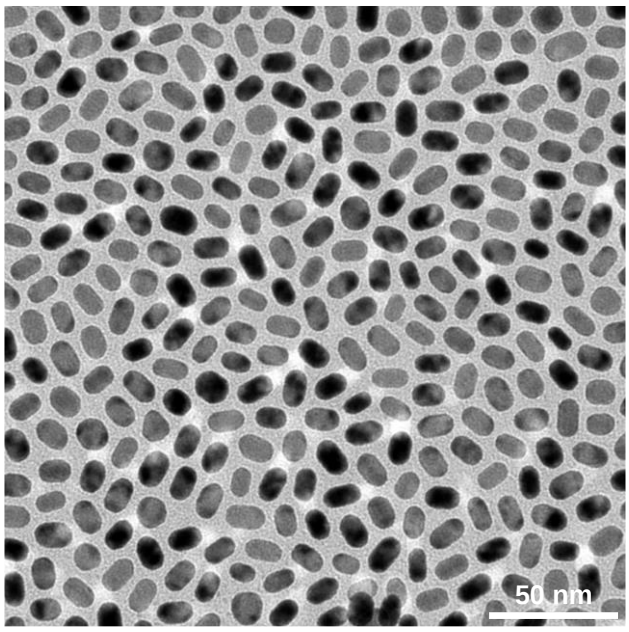


**Fig. S18.** TEM micrograph of produced $Pd_2Sn$-s NRs.

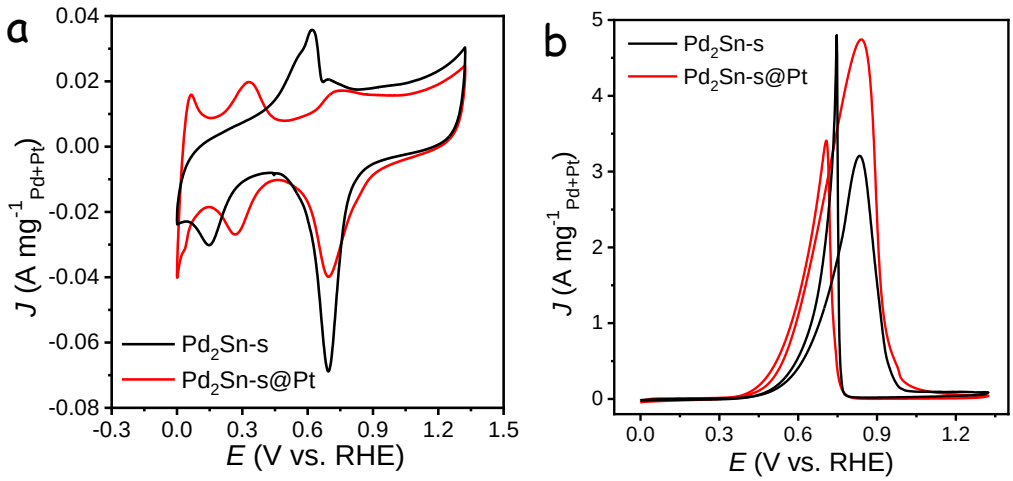


**Fig. S19.** (a) CV curves of $Pd_2Sn$-s and $Pd_2Sn$-s@Pt catalysts in a 1 M KOH electrolyte. (b) CV curves of $Pd_2Sn$-s and $Pd_2Sn$-s@Pt catalysts in a 1 M KOH + 1 M ethanol electrolyte.

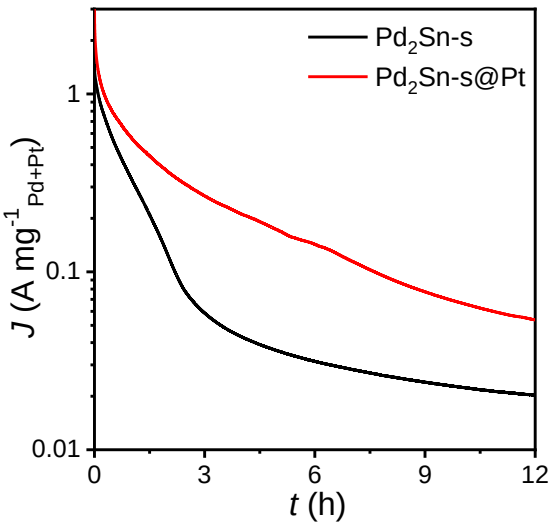


**Fig. S20.** CA curves of $Pd_2Sn$-s and $Pd_2Sn$-s@Pt catalysts in a 1 M KOH + 1 M ethanol electrolyte.

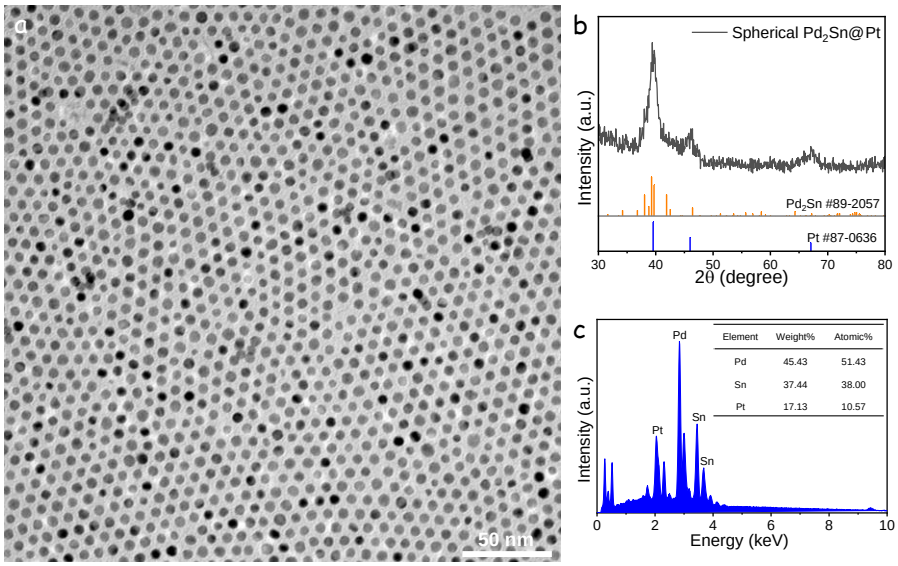


**Fig. S21.** (a) TEM micrograph, (b) XRD pattern and (c) EDS elemental composition of the produced spherical $Pd_2Sn$@Pt nanoparticles.

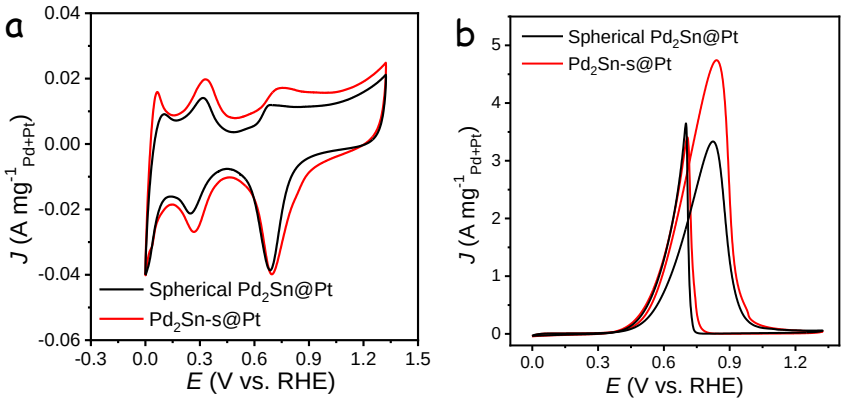


**Fig. S22.** (a) CV curves of spherical $Pd_2Sn$@Pt and $Pd_2Sn$-s@Pt catalysts in a 1 M KOH electrolyte. (b) CV curves of spherical $Pd_2Sn$@Pt and $Pd_2Sn$-s@Pt catalysts in a 1 M KOH + 1 M ethanol electrolyte.

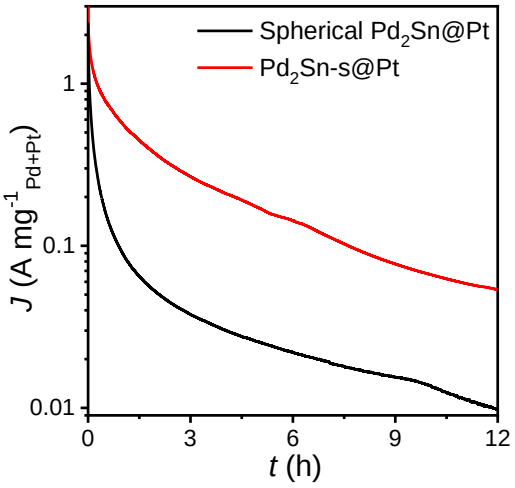


**Fig. S23.** CA curves of spherical $Pd_2Sn$@Pt and $Pd_2Sn$-s@Pt catalysts in a 1 M KOH + 1 M ethanol electrolyte.

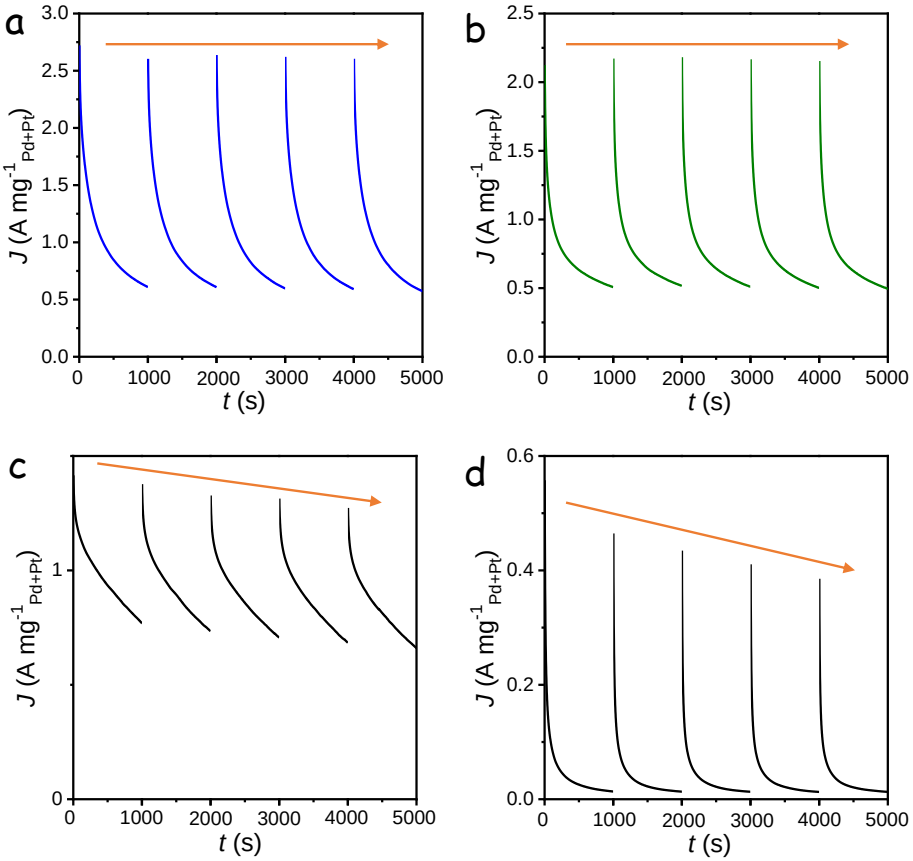


**Fig. S24.** CA curves of (a) $Pd_2Sn$-m@Pt, (b) $Pd_2Sn$-l@Pt, (c) $Pd_2Sn$-s and (d) Pt/C catalysts with CV reactivation every 1000s.

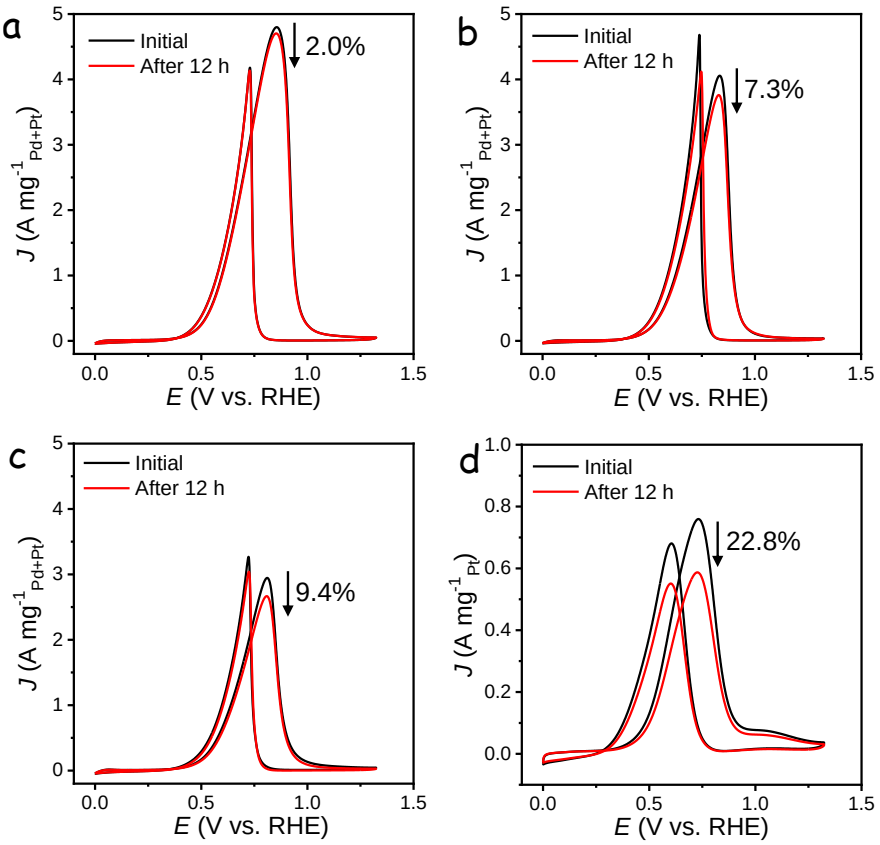


**Fig. S25.** CV curves before and after 12 h CA measurement with subsequent reactivation of (a) $Pd_2Sn$-s@Pt, (b) $Pd_2Sn$-m@Pt, (c) $Pd_2Sn$-l@Pt and (d) Pt/C catalysts.

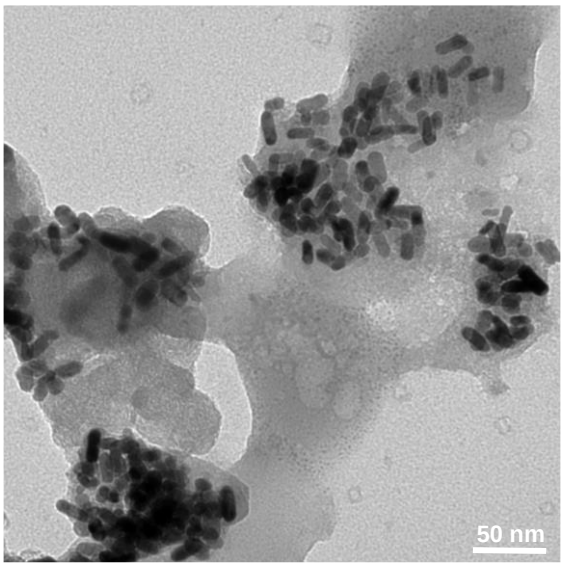


**Fig. S26.** TEM micrograph of $Pd_2Sn$-s@Pt catalyst after the stability measurement.

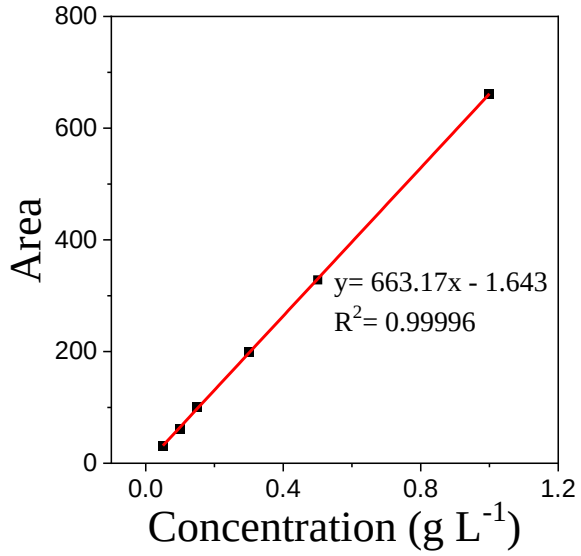


**Fig. S27.** The standard curves of acetic acid in HPLC.

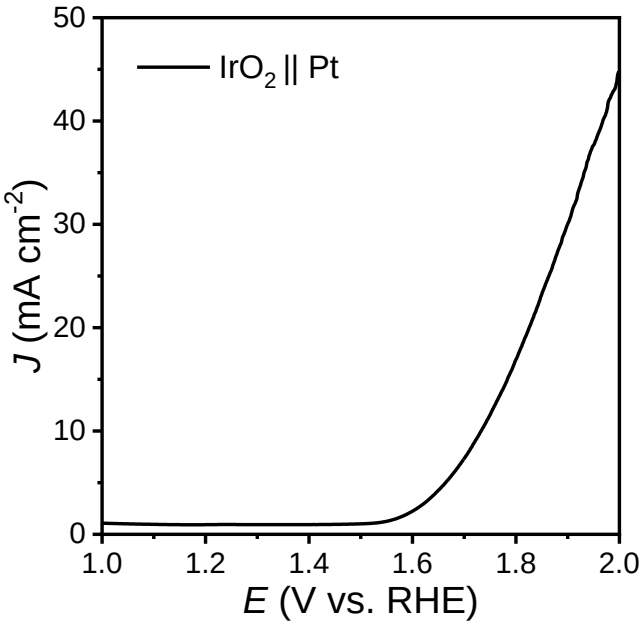


**Fig. S28.** LSV curve of the two electrolyzer system using $IrO_2$ as anode and Pt mesh as cathode in a 1 M KOH electrolyte.

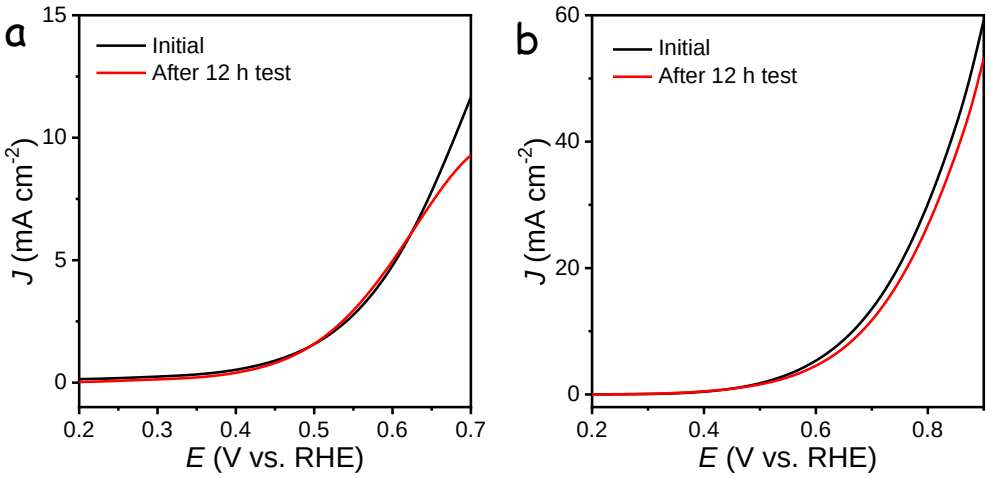


**Fig. S29.** LSV curve of (a) Pt/C || Pt and (b) $Pd_2Sn$-s || Pt electrolyzer system before and after 12 h CA measurement with subsequent reactivation.

**Table S1.** Comparison of activity of Pt or Pd-based catalysts for EOR.

| Catalysts | Electrolyte | Specific activity ($mA\ cm^{-2}$) | Mass activity ($A\ mg^{-1}$) | Stability (s) | Ref. |
|---|---|---|---|---|---|
| $Pd_2Sn$-s@Pt | 1 M KOH+1 M EtOH | 20.14 | 4.75 | 43200 | This work |
| PdPtAu | 0.1 M NaOH+0.1 M EtOH | 4.4 | 0.33 | 3600 | 9 |
| PtPd | 1 M KOH+1 M EtOH | 1.671 | 0.991 | 1000 | 10 |
| Au@Pt-Pd | 1 M KOH+1 M EtOH | 3.66 | 3.18 | - | 11 |
| PtIr | 1 M KOH+1 M EtOH | 10.22 | 4.18 | 3600 | 12 |
| PtIrNi | 1 M KOH+1 M EtOH | 5.2 | 3.8 | 1000 | 13 |
| $Pt_1Rh_1$ | 1 M KOH+1 M EtOH | 7.8 | 0.46 | 2000 | 14 |
| $Pt_3Rh_1Ni_2$ | 1 M NaOH+1 M EtOH | 7.97 | 1.39 | 1800 | 15 |
| PtPdRh | 1 M KOH+1 M EtOH | 1.37 | 1.35 | 1000 | 16 |
| SnPd | 1 M KOH+1 M EtOH | 5.72 | 3.8 | 36000 | 17 |
| PdBi | 1 M KOH+1 M EtOH | 4.33 | 3.21 | 3600 | 18 |
| PdAgAu | 1 M KOH+1 M EtOH | 5.5 | 2.39 | 4000 | 19 |
| PdRhTe | 1 M KOH+1 M EtOH | 6.53 | 2.04 | 3600 | 20 |
| PdBi | 1 M KOH+1 M EtOH | 10.37 | 3.5 | 3600 | 21 |
| PtRh@$SnO_2$ | 1 M NaOH+1 M EtOH | 5.63 | 3.16 | 1000 | 22 |
| TS-Pd/C | 1 M KOH+1 M EtOH | 3.22 | 1.846 | - | 23 |

**Table S2.** Comparison of the performance of two-electrolyzer hydrogen production system coupled with anodic small molecule oxidation.

| Catalysts | Oxidative substrates | Anodic product | Cell voltage (V) | Ref. |
|---|---|---|---|---|
| $Pd_2Sn$-s@Pt/C(+)\|\|Pt/C(-) | ethanol | acetic acid | 0.59 | This work |
| RhNiFe-P/NF(+)\|\|RhNiFe-P/NF(-) | ethanol | acetic acid | 1.42 | 24 |
| Co-S-P/CC(+)\|\|Co-S-P/CC(-) | ethanol | acetic acid | 1.63 | 25 |
| SA In-Pt NWs/C(+)\|\|SA In-Pt NWs/C(-) | ethanol | acetic acid | 0.62 | 26 |
| PtIr NWs/C(+)// PtIr NWs/C(-) | ethanol | 1,1-diethoxyethane | 0.61 | 27 |
| Ni–Mo–N/CFC(+) \|\| Ni–Mo–N/CFC(-) | glycerol | formate | 1.36 | 28 |
| NiVRu-LDHs/NF(+)\|\| NiVRu-LDHs/NF(-) | glycerol | formate | 1.35 | 29 |
| NiFe NSs/NF(+)\|\|Pt/C(-) | urea | $CO_2$+$N_2$ | 1.4 | 30 |
| RuCoP-NC(+)\|\|Pt/C(-) | urea | $CO_2$+$N_2$ | 1.33 | 31 |
| NiMoS(+)\|\|NiMoS(-) | urea | $CO_2$+$N_2$ | 1.384 | 32 |
| $Cu_{0.5}Ni_{0.5}$/NF(−) \|\| $Cu_{0.5}Ni_{0.5}$/NF(+) | urea | $CO_2$+$N_2$ | 1.38 | 33 |
| CuxO/CF(+)\|\|h-Ru-CuxO/CF(-) | ethylene glycol | formate | 1.25 | 34 |
| Ru/$Ni_2P$/NF(+)\|\|Ru/$Ni_2P$/NF(-) | ethylene glycol | $CO_2$ | 1.14 | 35 |
| Rh/RhOOH Metallene(+)\|\|Rh/RhOOH metallene(-) | ethylene glycol | glycolate | 0.678 | 36 |
| FeRu-MOF/NF(+)\|\|FeRu-MOF/NF(-) | methanol | formate | 1.4 | 37 |
| Pd@$Rh_{0.07}$Pd NDs(+)\|\|Pd@$Rh_{0.07}$Pd NDs(-) | methanol | $CO_2$ | 0.813 | 38 |
| Os–$Ni_x$P/N–C/NF(+)\|\|Os–$Ni_x$P/N–C/NF(-) | methanol | formate | 1.43 | 39 |
| CC/AN Pd(+)\|\|CC/AN Pd(-) | oxalic acid | $CO_2$ | 1.09 | 40 |
| RuCoMn@NC(+)\|\|RuCoMn@NC(-) | glucose | gluconate | 1.63 | 41 |

## References


[1] A. T. Fafarman, W. Koh, B. T. Diroll, D. K. Kim, D. K. Ko, S. J. Oh, X. Ye, V. Doan-Nguyen, M. R. Crump, D. C. Reifsnyder, C. B. Murray and C. R. Kagan, *J. Am. Chem. Soc.,* 2011, **133**, 15753–15761.

[2] G. Kresse and J. Hafner, Phys. Rev. B: Condens. *Matter Mater. Phys.,* 1993, **47**, 558– 561.

[3] G. Kresse and J. Furthmüller, *Comput. Mater. Sci.,* 1996, **6**, 15– 50.

[4] J. P. Perdew and K. Burke, *Phys. Rev. Lett.,* 1996, **77**, 3865– 3868.

[5] J. P. Perdew and Y. Wang, Phys. Rev. B: Condens. *Matter Mater. Phys.,* 1992, **45**, 13244.

[6] P. E. Blöchl, Phys. Rev. B: Condens. *Matter Mater. Phys.,* 1994, **50**, 17953– 17979.

[7] S. Grimme, J. Antony, S. Ehrlich and H. Krieg, *J. Chem. Phys.,* 2010, **132**, 154104.

[8] S. Grimme, S. Ehrlich and L. Goerigk, *J. Comput. Chem.,* 2011, **32**, 1456– 1465.

[9] J. Tang, N. Tian, L. Xiao, Q. Chen, Q. Wang, Z. Zhou and S. Sun, *J. Mater. Chem. A,* 2022, **10**, 10902–10908.

[10] C. Liu, X. Ran, G. Li, Z. Li, G. Du, L. Yang, L. Li and Q. Qu, *Int. J. Hydrog. Energy,* 2023, S0360319923010686.

[11] W. Liang, Y. Wang, L. Zhao, W. Guo, D. Li, W. Qin, H. Wu, Y. Sun and L. Jiang, *Adv. Mater.,* 2021, **33**, 2100713.

[12] Y. Fang, S. Guo, D. Cao, G. Zhang, Q. Wang, Y. Chen, P. Cui, S. Cheng and W. Zuo, *Nano Res.,* 2022, **15**, 3933–3939.

[13] Y. H. Ahmad, A. T. Mohamed, K. M. Youssef, S. Kundu, K. A. Mkhoyan and S. Y. Al-Qaradawi, *Electrochem. Commun.,* 2019, **101**, 61–67.

[14] J. Bai, X. Xiao, Y. Xue, J. Jiang, J. Zeng, X. Li and Y. Chen, *ACS Appl. Mater. Interfaces,* 2018, **10**, 19755–19763.

[15] H. Liu, J. Li, L. Wang, Y. Tang, B. Y. Xia and Y. Chen, *Nano Res.,* 2017, **10**, 3324–3332.

[16] C. Liu, T. Wu, F. Zeng, X. Pan, G. Li, K. Teng, X. Ran, Q. Qu, L. Li and L. Yang, *Electrochim. Acta,* 2023, **437**, 141531.

[17] D. Liu, S. Tian, Y. Zhang, C. Hu, H. Liu, D. Chen, L. Xu and J. Yang, *ACS Appl. Energy Mater.,* 2023, **6**, 1459–1466.

[18] Y. Wang, M. Li, Z. Yang, W. Lai, J. Ge, M. Shao, Y. Xiang, X. Chen and H. Huang, *Mater. Horiz.,* 2023, **10**, 1416–1424.

[19] H. Wang, S. Jiao, S. Liu, K. Deng, H. Yu, X. Wang, Y. Xu, Z. Wang and L. Wang, *J. Mater. Chem. A,* 2022, **10**, 24051–24055.

[20] L. Jin, H. Xu, C. Chen, H. Shang, Y. Wang and Y. Du, *Inorg. Chem.,* 2019, **58**, 12377–12384.

[21] X. Li, H. You, C. Wang, D. Liu, R. Yu, S. Guo, Y. Wang and Y. Du, *J. Colloid Interface Sci.,* 2021, **591**, 203–210.

[22] X. Fan, M. Tang, X. Wu, S. Luo, W. Chen, X. Song and Z. Quan, *J. Mater. Chem. A,* 2019, **7**, 27377–27382.

[23] C. Liu, Y. Shen, J. Zhang, G. Li, X. Zheng, X. Han, L. Xu, S. Zhu, Y. Chen, Y. Deng and W. Hu, *Adv. Energy Mater.,* 2022, **12**, 2103505.

[24] J. Miao, X. Zhao, H.-Y. Hu, H. Huang, Y. Ding, Z.-H. Liu and Y. Chen, *ACS Appl. Nano Mater.,* 2022, **5**, 4948–4957.

[25] S. Sheng, K. Ye, L. Sha, K. Zhu, Y. Gao, J. Yan, G. Wang and D. Cao, *Inorg. Chem. Front.,* 2020, **7**, 4498–4506.

[26] Y. Zhu, X. Zhu, L. Bu, Q. Shao, Y. Li, Z. Hu, C. Chen, C. Pao, S. Yang and X. Huang, *Adv. Funct. Mater.,* 2020, **30**, 2004310.

[27] K. Yin, Y. Chao, F. Lv, L. Tao, W. Zhang, S. Lu, M. Li, Q. Zhang, L. Gu, H. Li and S. Guo, *J. Am. Chem. Soc.,* 2021, **143**, 10822–10827.

[28] Y. Li, X. Wei, L. Chen, J. Shi and M. He, *Nat. Commun.,* 2019, **10**, 5335.

[29] Q. Qian, X. He, Z. Li, Y. Chen, Y. Feng, M. Cheng, H. Zhang, W. Wang, C. Xiao, G. Zhang and Y. Xie, *Adv. Mater.,* 2023, 2300935.

[30] Y. Diao, Y. Liu, G. Hu, Y. Zhao, Y. Qian, H. Wang, Y. Shi and Z. Li, *Biosens. Bioelectron.,* 2022, **211**, 114380.

[31] L. Gu, Y. Li and A. D. Chowdhury, *Mater. Today Chem,* 2023, **27**, 101290.

[32] Y. Fang, M. Li, X. Guo, Z. Duan and A. Safikhani, *Int. J. Hydrog. Energy,* 2023, S0360319923006936.

[33] K. Zhang, S. Wang, X. Li, H. Li and Y. Ni, *Small,* 2023, 2300959.

[34] L. Liu, Y. He, D. Ma, X. Wu and Q. Zhu, *J. Colloid Interface Sci.,* 2023, **640**, 423–433.

[35] G. Ma, N. Yang, Y. Xue, G. Zhou and X. Wang, *ACS Appl. Mater. Interfaces,* 2021, **13**, 42763–42772.

[36] Q. Mao, K. Deng, H. Yu, Y. Xu, Z. Wang, X. Li, L. Wang and H. Wang, *Adv. Funct. Mater.,* 2022, **32**, 2201081.

[37] Q. Ling, Z. Zhao, Z. Li, K. Yan, C. Ding, P. Chen, Z. Sun, G. He, J. Lv and M. Zhang, *J. Mater. Chem. A,* 2023, **11**, 2876–2888.

[38] Y. Jiang, H. Sun, Y. Li, J. He, Q. Xue, X. Tian, F. Li, S. Yin, D. Li and Y. Chen, *ACS Appl. Mater. Interfaces,* 2021, **13**, 35767–35776.

[39] Z. Duan, T. Ren, Q. Mao, H. Yu, K. Deng, Y. Xu, Z. Wang, L. Wang and H. Wang, *J. Mater. Chem. A,* 2022, **10**, 18126–18131.

[40] Y. Wang, J. Su, L. Zhang, Y. Liu, X. Miao, J. Liu, Q. Li, L. Ding and Y. Tang, *Int. J. Hydrog. Energy,* 2023, S0360319923012946.

[41] S. Liu, E. Zhang, X. Wan, R. Pan, Y. Li, X. Zhang, M. Su, J. Liu and J. Zhang, *Sci. China Mater.,* 2022, **65**, 131–138.